PHOTONICS Research

Multiple conical odd harmonics from filament-inscribed nanogratings

Robertas Grigutis, Vytautas Jukna, Gintaras Tamošauskas, and Audrius Dubietis*

Laser Research Center, Vilnius University, LT-10223 Vilnius, Lithuania
**Corresponding author: audrius.dubietis@ff.vu.lt*

Received 26 April 2023; revised 4 August 2023; accepted 21 August 2023; posted 23 August 2023 (Doc. ID 494150); published 9 October 2023

We report on the observation of conical third, fifth, seventh, and ninth harmonics that gradually emerge during the supercontinuum generation by filamentation of femtosecond midinfrared pulses in lithium strontium hexafluoroaluminate crystal. We show that the generation of conical odd harmonics is an optical signature of light-driven material reorganization in the form of volume nanogratings at the site irradiated by repetitive femtosecond filaments. The angle-resolved spectral measurements demonstrate remarkably broad spectra of individual odd harmonics, benefiting from a spectrally broadened pump pulse (supercontinuum), and reveal that filament-inscribed nanogratings represent photonic structures that are able to provide ultrabroad phase-matching bandwidths covering the wavelength range from the ultraviolet to the near infrared. We propose a scenario that interprets the generation of conical fifth, seventh, and ninth harmonics as nanograting phase-matched cascaded noncollinear four-wave mixing processes.

https://doi.org/10.1364/PRJ.494150

1. INTRODUCTION

Ultrafast nonlinear interactions of ultrashort laser pulses with transparent materials unveil rich physics, which attracts a great deal of interest from the fundamental and applied science. Femtosecond filamentation represents the most outstanding example of laser–matter interactions from the perspective of light [1], resulting in large-scale spectral broadening, termed "supercontinuum generation" [2,3]. Due to its high degree of spatial and temporal coherence [4], bulk-generated supercontinuum represents a unique ultrafast broadband source that currently serves as an important asset to the design of broadly tunable optical parametric amplifiers [5], optical parametric chirped pulse amplifiers [6], few-cycle pulse generation, pulse post-compression techniques [7], wave-form synthesis [8], and time-resolved spectroscopy [9,10]. From the material perspective, irradiation by repetitive laser pulses leads to local modification of the material structure and the electronic properties in three dimensions, opening the perspectives for laser processing of transparent materials, refractive index engineering, and integrated photonics [11–14].

These two research directions pursue fundamentally opposite tasks and use different strategies of implementation. In contrast with laser material processing-oriented applications, which seek controllable light-driven material reorganization, supercontinuum generation aims at modification-free performance of the nonlinear material. However, these two aspects of laser-matter interaction inevitably collide when the transparent material is irradiated with high-repetition-rate laser pulses. In that way, every subsequent laser pulse starts seeing slightly modified nonlinear materials by the propagation of previous pulses, and this modification evolves in a runaway manner with an increasing number of impinging pulses. As a result, the light-driven material reorganization emerges in the form of self-organized (quasi) periodic nanogratings in the volume of transparent materials [15–17]. The buildup of such periodic structures in turn affects the nonlinear propagation of the laser pulse, altering filamentation dynamics that result in shrinking of the supercontinuum spectrum but at the same time give rise to nonlinear optical side effects such as conical third-harmonic generation [18]. More specifically, the third harmonic is generated along the cone, whose angle is defined by the longitudinal phase-matching set by material dispersion, whereas the transverse phase-matching is achieved by means of reciprocal lattice vector inversely proportional to the period of nanograting that yields appropriate periodic modulation of cubic nonlinear susceptibility [19]. The universality of nanograting-phase-matched conical third-harmonic generation was justified by the observations of this phenomenon in various transparent materials [20]. More recently, it was demonstrated that volume nanogratings inscribed by light filaments with central wavelengths that fall into the region of anomalous group velocity dispersion of the material, provide ultrabroad phase-matching bandwidths, resulting in conical third-harmonic generation with octave-spanning spectra [21]. In general, third-harmonic generation readily serves as an optical signature of material structural modification [22] and could be used for *in situ*

monitoring of femtosecond laser processing of bulk dielectrics [23].

In this paper, we report on simultaneous generation of conical third, fifth, seventh, and ninth harmonics from volume nanogratings inscribed in lithium strontium hexafluoroaluminate (LiSAF) crystal by filamentation of 200 fs, 2.5 μm pulses. We show that filament-inscribed nanogratings represent photonic structures that are able to provide ultrabroad phase-matching bandwidths covering wavelength range from the ultraviolet to the near infrared and propose the odd harmonics generation scenario that is based on phase-matched cascaded noncollinear four-wave mixing processes.

2. EXPERIMENTAL DETAILS

Lithium strontium hexafluoroaluminate (LiSAF) crystal was chosen as the nonlinear material in our experiments. Broad transparency range and relatively low chromatic dispersion make this crystal suitable for supercontinuum generation in the ultraviolet with either ultraviolet or visible pumping; on the other hand, the crystal optically degrades with pumping in the infrared due to increased role of impact ionization at longer wavelengths [24]. Bearing in mind the latter issue, in the present work we studied the nonlinear propagation of 200 fs pulses with a central wavelength of 2.5 μm, produced by an optical parametric amplifier (OPA, Orpheus-ONE-HP, Light Conversion Ltd.), which was pumped by the fundamental harmonic of an amplified Yb:KGW laser (Pharos, Light Conversion Ltd.) operating at 2 kHz repetition rate. The OPA beam of 1.9 mm diameter (at the $1/e^2$ intensity level) was focused with an $f = +30$ mm lens onto the front face of a 5 mm long uncoated and undoped LiSAF sample. The input pulse energy of 10.4 μJ was set to induce a single filament that in turn produced broadband supercontinuum with a spectral blueshift extending up to 390 nm, as measured at the center of the beam. All the spectral measurements were performed with a minispectrometer (Qmini VIS-LC, Broadcom Inc.) with a detection range of 293–1115 nm. The spectrometer was mounted on a motorized rotating arm for recording the angle-resolved spectra of the entire emission pattern produced at the crystal output (see Ref. [21] for more details). The (average) power measurements of individual harmonics were performed with calibrated photodiodes using a set of appropriate bandpass filters. The crystal was kept in a stationary position during the entire session of either spectral or power measurements, thus allowing for precisely capturing the evolution of relevant features of supercontinuum and harmonics emissions, associated with formation of filament-inscribed nanogratings.

3. RESULTS AND DISCUSSION

Figure 1 shows the screenshots of emission patterns recorded at different moments of time and representing the relevant experimental findings in a nutshell. At the beginning, filamentation of the input beam produces supercontinuum and conical emission that appear as a wide bright spot [see Fig. 1(a)]. Such an image is typically observed in any supercontinuum generation experiment, where the generated spectrum spans over the whole visible spectral range.

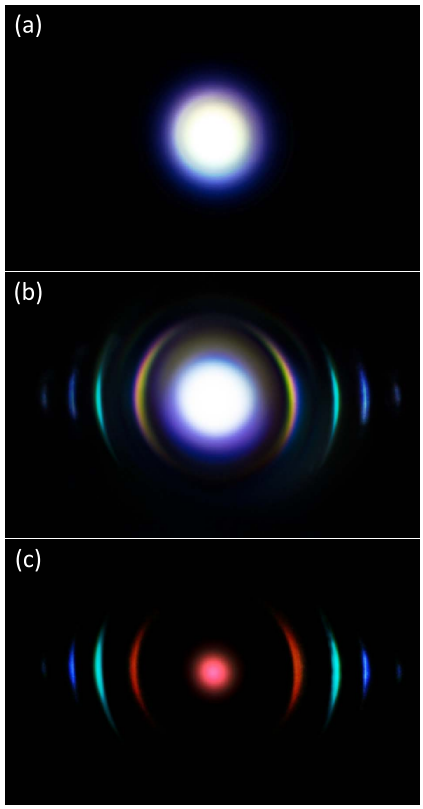

Fig. 1. Emission patterns at the output of the crystal, recorded (a) at the very beginning of the experiment and after (b) 1 h and (c) 2.4 h of exposure time.

Shortly (after a few tens of seconds), there gradually emerges an array of concentric half-rings of different colors, which are attributed to conical odd harmonics. Figure 1(b) shows the representative image of the emission pattern taken after 1 h of exposure time. The innermost half-ring represents the conical third harmonic, which, despite its infrared (833 nm) central wavelength, becomes visible due to its broad spectrum. The middle blue-green half-ring is attributed to the conical fifth harmonic, whose central wavelength falls into the visible range (500 nm), while the outermost fainter half-rings are attributed to the conical seventh and ninth harmonics with center wavelengths of 357 and 278 nm, respectively, which are visualized through blue luminescence of the paper screen. Note the alignment of harmonics half-rings along the horizontal axis in the plane of view, suggesting that the filament-inscribed nanograting is preferentially oriented perpendicular to the polarization direction of the input pulse (that is vertical in the plane of view). Finally, the central spot visually shrinks in dimension and changes its color to red [see the image in Fig. 1(c)], which was taken after 2.4 h of exposure time, indicating the extinction of the supercontinuum, and what remains visible at the center is just a signal of the collinear phase-mismatched third harmonic. Note also an apparent change of color of the conical third harmonic ring; all these features will be discussed later in more detail with presentation of angle-resolved spectra.

Figure 2 presents the measured harmonics' powers as functions of exposure time, demonstrating almost immediate

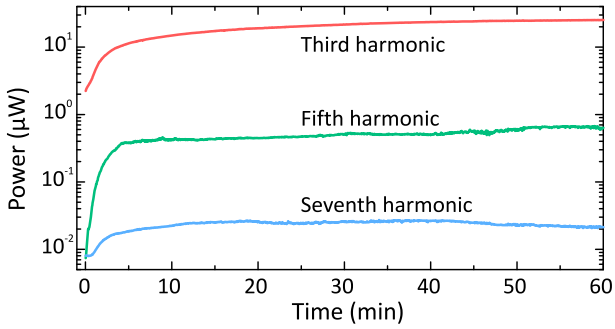

Fig. 2. Measured average powers of conical third, fifth, and seventh harmonics as functions of exposure time.

(after a few tens of seconds) emergence of conical third, fifth, and seventh harmonics. Here, the power of the ninth harmonic was not measured due to its low signal-to-noise ratio. During the first few minutes of exposure, the harmonics' powers experience rapid growth until they settle after approximately 5 min and thereafter remain almost constant during the remaining measurement time. The measured power trends attest the onset, buildup, and stabilization of nanogratings inscribed by a light filament and provide the characteristic time scales of their development stages. The estimated steady powers of third, fifth, and seventh harmonics were 25 μW, 500 nW, and 25 nW, respectively, yielding the corresponding conversion efficiencies of 1.2×10^{-3}, 2.4×10^{-5}, and 1.2×10^{-6}, assuming the input power of 20.7 mW at the fundamental wavelength (the input pulse energy of 10.4 μJ and pulse repetition rate of 2 kHz). Relatively low values of harmonics powers and conversion efficiencies could be explained by a rather complicated interaction geometry. Although the harmonics are continuously generated along the entire nanograting, whose length may approach the length of a light filament, the local overlap of the interacting beams is reduced to just a few micrometers, assuming relatively large propagation angles of individual harmonics and an approximate diameter of a light filament of 5 μm at full width at half maximum [1].

Figure 3 presents the angle-resolved spectra of the output radiation recorded at three different moments of time. Figure 3(a) shows the angle-resolved spectrum of the output radiation recorded during the buildup stage of a nanograting (after 3 min of exposure time). The strong broadband emission on and close to the beam propagation axis is attributed to the blueshifted portion of the supercontinuum, which ends with an intense blue peak centered at around 425 nm and a characteristic angular spread of the most blueshifted spectral components resembling a "fish-tail" that comprises the conical emission. The parasitic spectral peak at 1030 nm is attributed to the leakage of the fundamental laser harmonic that served as the OPA pump. The conical third, fifth, and seventh harmonics with central wavelengths of 833, 500, and 357 nm, respectively, are clearly distinguishable, as they emerge at relatively large angles, which increase with the increasing harmonics order. Although the central wavelength of the ninth harmonic (278 nm) is outside the short-wavelength detection limit (293 nm) of the spectrometer, its faint most-redshifted

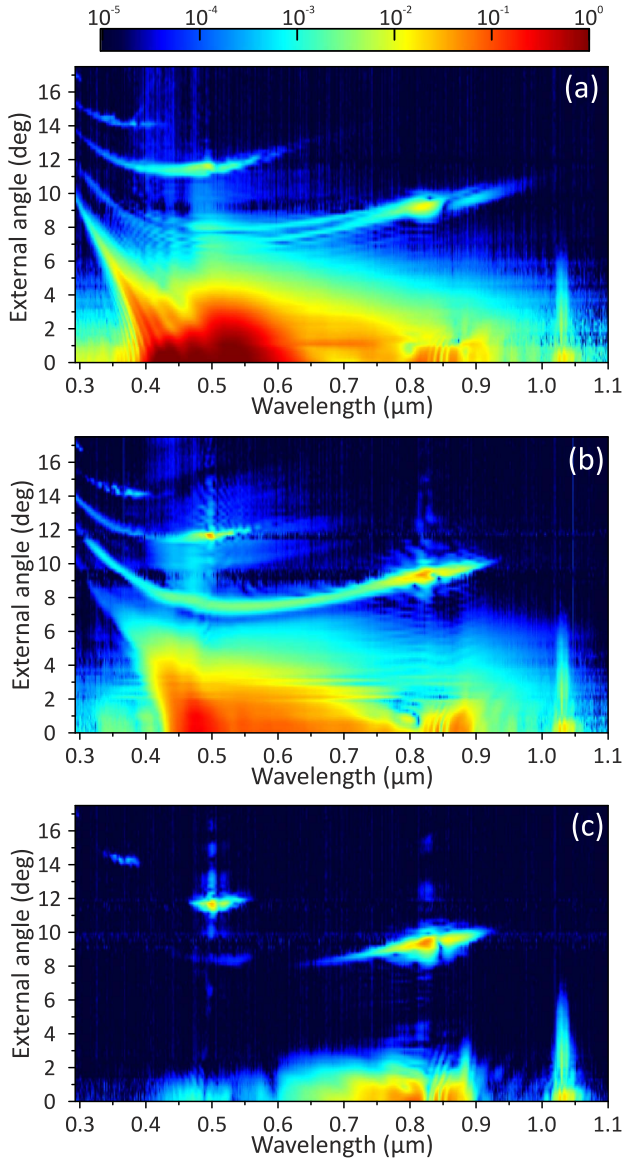

Fig. 3. Angle-resolved spectra of supercontinuum and harmonics emissions measured after (a) 3 min, (b) 1 h, and (c) 4 h of exposure time.

spectral components are readily detectable at the top of left corner of the plot. A distinctive feature of individual odd harmonics spectra is their remarkably broad bandwidths. The spectrum of third harmonic extends from the ultraviolet to the near-infrared (310–950 nm); the coloration of its visible part is readily discernible in Fig. 1(b) due to the differences of phase-matching angles for different spectral components of a broadband fundamental pulse (see Ref. [21] for more details). Such a broadband third-harmonic spectrum is produced by frequency tripling of spectrally broadened driving pulse (more specifically, its near- to midinfrared part in the wavelength range of 0.93–2.85 μm), which is outside the detection range. Higher-order harmonics exhibit notably broad spectral bandwidths as well: the spectrum of the fifth harmonic covers a large part of the visible range (up to 600 nm) and extends to

below 300 nm, and the spectrum of seventh harmonic is in the 310–480 nm range.

The angle-resolved spectrum measured after 1 h of exposure time (after harmonics powers have long been settled) is shown in Fig. 3(b) and demonstrates essentially identical angular distributions of harmonics spectra with increased intensities. However, the changes occur in the supercontinuum spectrum, whose blue peak gradually shifts toward the long-wavelength side (centered at ~480 nm in the present case) and continues to do so with the increase of exposure time.

The angle-resolved spectrum measured after 4 h of exposure time is presented in Fig. 3(c) and shows how the spectra of individual harmonics shrink significantly due to extinction of the supercontinuum spectrum. Indeed, the supercontinuum signal in the visible and near-infrared spectral range completely ceases, unveiling the signal of the collinear phase-mismatched third harmonic with a central wavelength of 833 nm and broadband spectrum, which on the short wavelength side extends into the visible range, thus becoming visible as a red central spot in Fig. 1(c). Note also that we uncovered a much weaker broadband signal in the 420–580 nm range, which is attributed to the collinear phase-mismatched fifth harmonic, which is produced via cascaded four-wave mixing between the fundamental and third harmonics [25]. Note that the propagation angles of individual conical harmonics increase with harmonics order, thus ruling out the possibility that the conical harmonics can be interpreted as a simple diffraction of their phase-mismatched axial counterparts by a filament-inscribed nanograting, which would yield the opposite distribution of angles (smaller diffraction angles for shorter wavelengths). The changes of spectral widths of individual harmonics are summarized in Fig. 4, which compares the angle-integrated spectra of conical harmonics measured after 1 and 4 h of exposure time.

Figure 5 presents the time evolutions of angle-integrated spectra of conical third and fifth harmonics in more detail. Note simultaneous narrowing of both harmonics spectra, which in turn correlates with shrinking of the near-infrared part of supercontinuum spectrum, demonstrating how the inscription of a nanograting along the filament path alters filamentation dynamics, which in turn affects spectral broadening and

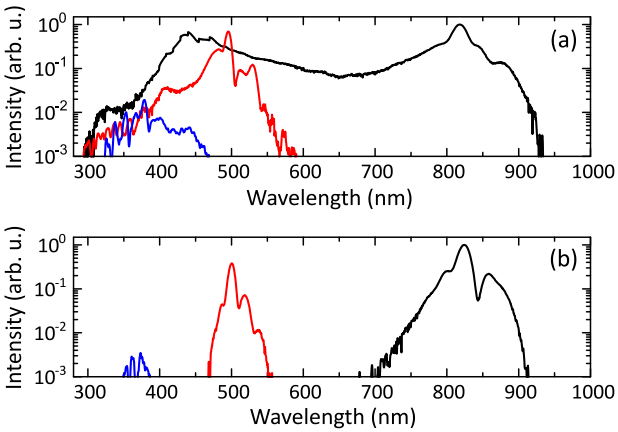

Fig. 4. Angle-integrated spectra of conical third (black curves), fifth (red curves), and seventh (blue curves) harmonics measured after (a) 1 h and (b) 4 h of exposure time.

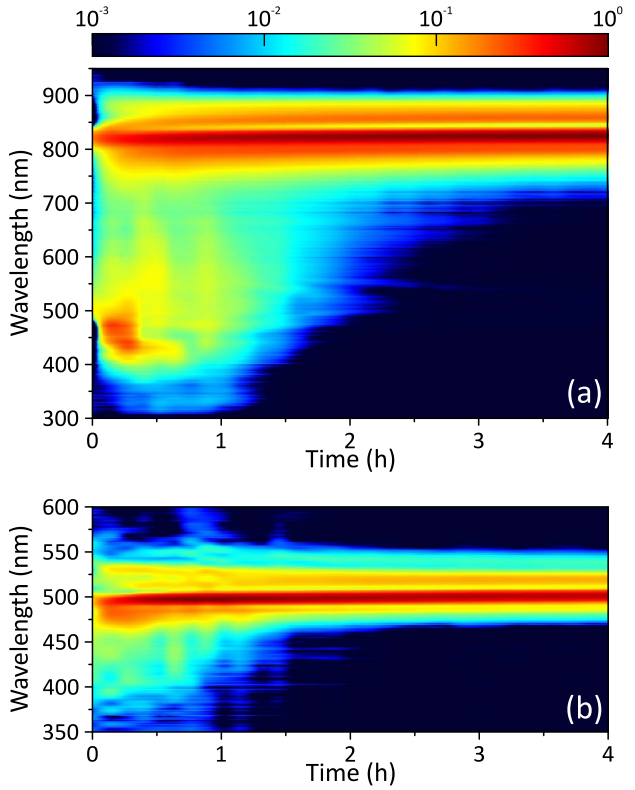

Fig. 5. Time evolutions of angle-integrated (a) third-harmonic and (b) fifth-harmonic spectra.

supercontinuum generation. The observed narrowing of harmonics spectra therefore is a clear signature of supercontinuum extinction, which eventually turns just into modest spectral broadening around the carrier wavelength of the input pulse (2.5 μm).

Figure 6(a) shows a representative example of the output pattern in the far field consisting of multiple half-rings attributed to conical third, fifth, seventh, and ninth harmonics. Figures 6(b)–6(e) depict the wave-vector diagrams illustrating the noncollinear phase-matching conditions for the generation of conical odd harmonics as cascaded four-wave interactions. Considering third-harmonic generation as a phase-matched noncollinear four-wave mixing process, as depicted in Fig. 6(b), the fifth-harmonic generation is then considered as a cascaded process that involves four-wave mixing between the fundamental and third harmonics, as shown in Fig. 6(c). Following this scenario, the seventh harmonic is generated via cascaded four-wave mixing between the fundamental and fifth harmonics [see Fig. 6(d)], while the ninth harmonic is generated via cascaded four-wave mixing between the fundamental and seventh harmonics, as shown in Fig. 6(e). The phase-matching conditions for the above processes read as

$$\begin{aligned} k_3 &= 3k_1 + G_3, \\ k_5 &= k_3 + 2k_1 + G_5, \\ k_7 &= k_5 + 2k_1 + G_7, \\ k_9 &= k_7 + 2k_1 + G_9, \end{aligned} \tag{1}$$

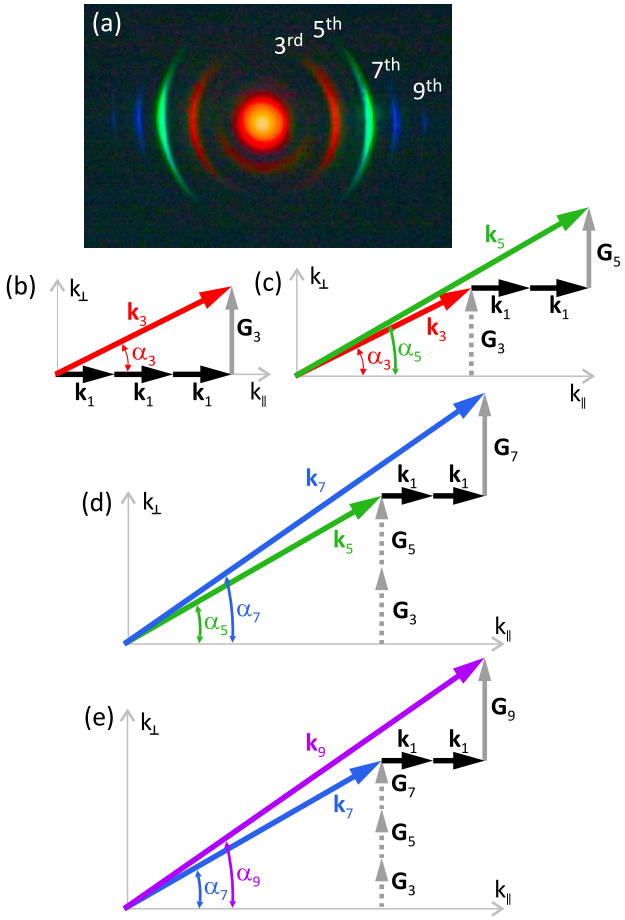

Fig. 6. (a) Intensified image showing angular distribution of conical odd harmonics. Wave-vector diagrams for the generation of (b) third, (c) fifth, (d) seventh, and (e) ninth conical harmonics.

where $k_i = \omega_i n_i/c$ and $G_i = 2\pi/\Lambda_i$ are the lengths of the wave vectors and reciprocal lattice vectors, respectively, with the subscripts indicating the harmonics order ($i = 1, 3, 5, 7, 9$). n_i denotes the corresponding refractive index, and Λ_i stands for the nanograting period, which might be different to phase-match different harmonics. Considering the above interaction geometries, the following expressions for the harmonics cone angles (α_i) and nanograting periods are derived:

$$\begin{aligned}\cos\alpha_3 &= \frac{n_1}{n_3},\\ \cos\alpha_5 &= \frac{n_1}{n_5},\\ \cos\alpha_7 &= \frac{n_1}{n_7},\\ \cos\alpha_9 &= \frac{n_1}{n_9},\end{aligned} \tag{2}$$

and

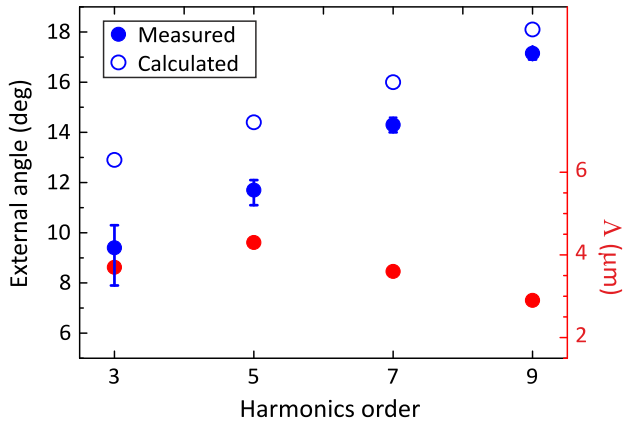

Fig. 7. Measured and calculated harmonics external cone angles (blue) and calculated nanograting periods (red).

$$\begin{aligned}\Lambda_3 &= \left(\frac{\sqrt{n_3^2 - n_1^2}}{\lambda_3}\right)^{-1},\\ \Lambda_5 &= \left(\frac{\sqrt{n_5^2 - n_1^2}}{\lambda_5} - \frac{1}{\Lambda_3}\right)^{-1},\\ \Lambda_7 &= \left(\frac{\sqrt{n_7^2 - n_1^2}}{\lambda_7} - \frac{1}{\Lambda_3} - \frac{1}{\Lambda_5}\right)^{-1},\\ \Lambda_9 &= \left(\frac{\sqrt{n_9^2 - n_1^2}}{\lambda_9} - \frac{1}{\Lambda_3} - \frac{1}{\Lambda_5} - \frac{1}{\Lambda_7}\right)^{-1},\end{aligned} \tag{3}$$

where λ_i ($i = 3,\ 5,\ 7,\ 9$) denotes the harmonics' wavelength. The calculated harmonics' cone angles inside the medium thereafter were converted to angles in the air using Snell's law and compared with the measured cone angles of third to ninth harmonics in Fig. 7. The error bars to experimental data points represent the angular widths of harmonic cones. Note that the calculated cone angles are systematically by a few degrees larger than the measured ones, and we attribute this discrepancy to imperfect knowledge of material dispersion. More specifically, the theoretical cone angles and respective nanograting periods were computed using the dispersion equation of LiSAF, which is valid only in the 0.4–1.2 μm range [26] and was therefore extrapolated to cover the entire wavelength range of interest, 0.275–2.6 μm. In fact, the extrapolation might produce large deviations of the so-calculated refractive index from its real values, in particular for what concerns the knowledge of n_1, which appears in all expressions of cone angles and nanograting periods [see Eqs. (2) and (3)]. Nevertheless, the estimated approximate period values seem feasible, bearing in mind that the period of inscribed structures is of the order of inscription wavelength. Note that there may be several other possible four-wave mixing configurations for the seventh- and ninth-harmonics generation, e.g., the seventh harmonic could be produced through the process $k_7 = 2k_3 + k_1 + G_7$ and the ninth harmonic as $k_9 = k_5 + k_3 + k_1 + G_9$. However, in the present case, we assumed that the most efficient process is the four-wave interaction that involves a larger number (two instead of one) of fundamental (the most intense) waves.

The proposed scenario of conical odd harmonics generation via cascaded four-wave mixing processes relies on light-induced permanent structural modification of the material. This is in contrast with the observations of conical third-harmonic generation in isotropic materials under tight focusing of the pump beam via higher-order, e.g., quintic nonlinearity [27,28]. On the other hand, the proposed scenario resembles to some extent the scenario underlying the simultaneous generation of second up to fifth harmonic conical beams by means of multistep second-order cascade processes in a 2D nonlinear photonic crystal ($LiNbO_3$) with periodically inverted hexagonal ferroelectric domains, making it possible to simultaneously satisfy a large number of quasiphase-matching conditions for three-wave interactions [29].

4. CONCLUSIONS

In conclusion, we demonstrated simultaneous generation of conical third, fifth, seventh, and ninth harmonics from volume nanogratings inscribed in LiSAF crystal by femtosecond midinfrared filaments. The relevant development stages of filament-inscribed nanogratings, i.e., onset, rapid buildup, and stabilization, are captured by the measurements of individual harmonics' powers as functions of laser exposure time. The spectra of individual harmonics exhibit remarkably broad bandwidths, attesting that filament-inscribed nanogratings provide ultrabroadband phase-matching bandwidths extending from the ultraviolet to the near-infrared. We propose the scenario that interprets the generation of conical fifth, seventh, and ninth harmonics as nanograting-phase-matched cascaded noncollinear four-wave mixing processes that are validated by the measurements of cone angles of individual harmonics and supported by the estimations of fundamental-to-individual harmonics conversion efficiencies.

Funding. Lietuvos Mokslo Taryba (S-MIP-22-40).

Disclosures. The authors declare no conflicts of interest.

Data Availability. Data underlying the results presented in this paper are not publicly available at this time but may be obtained from the authors upon reasonable request.

REFERENCES

1. A. Couairon and A. Mysyrowicz, "Femtosecond filamentation in transparent media," Phys. Rep. **441**, 47–189 (2007).
2. A. Dubietis, G. Tamošauskas, R. Šuminas, V. Jukna, and A. Couairon, "Ultrafast supercontinuum generation in bulk condensed media," Lith. J. Phys. **57**, 113–157 (2017).
3. A. Dubietis and A. Couairon, *Ultrafast Supercontinuum Generation in Transparent Solid State Media* (Springer, 2019).
4. A. Halder, V. Jukna, M. Koivurova, A. Dubietis, and J. Turunen, "Coherence of bulk-generated supercontinuum," Photon. Res. **7**, 1345–1353 (2019).
5. C. Manzoni and G. Cerullo, "Design criteria for ultrafast optical parametric amplifiers," J. Opt. **18**, 103501 (2016).
6. A. Dubietis and A. Matijošius, "Table-top optical parametric chirped pulse amplifiers: past and present," Opto-Electron. Adv. **6**, 220046 (2023).
7. T. Nagy, P. Simon, and L. Veisz, "High-energy few-cycle pulses: post-compression techniques," Adv. Phys. X **6**, 1845795 (2021).
8. G. Cirmi, R. E. Mainz, M. A. Silva-Toledo, F. Scheiba, H. Çankaya, M. Kubullek, G. M. Rossi, and F. X. Kärtner, "Optical waveform synthesis and its applications," Laser Photonics Rev. **17**, 2200588 (2023).
9. N. Krebs, I. Pugliesi, J. Hauer, and E. Riedle, "Two-dimensional Fourier transform spectroscopy in the ultraviolet with sub-20 fs pump pulses and 250–720 nm super-continuum probe," New J. Phys. **15**, 085016 (2013).
10. F. Vernuccio, A. Bresci, B. Talone, A. De La Cadena, C. Ceconello, S. Mantero, C. Sobacchi, R. Vanna, G. Cerullo, and D. Polli, "Fingerprint multiplex CARS at high speed based on supercontinuum generation in bulk media and deep learning spectral denoising," Opt. Express **30**, 30135–30148 (2022).
11. M. Beresna, M. Gecevičius, and P. G. Kazansky, "Polarization sensitive elements fabricated by femtosecond laser nanostructuring of glass [Invited]," Opt. Mater. Express **1**, 783–795 (2011).
12. S. Richter, M. Heinrich, S. Döring, A. Tünnermann, S. Nolte, and U. Peschel, "Nanogratings in fused silica: formation, control, and applications," J. Laser Appl. **24**, 042008 (2012).
13. R. Stoian and J.-P. Colombier, "Advances in ultrafast laser structuring of materials at the nanoscale," Nanophotonics **9**, 4665–4688 (2020).
14. R. Stoian, "Volume photoinscription of glasses: three-dimensional micro- and nanostructuring with ultrashort laser pulses," Appl. Phys. A **126**, 438 (2020).
15. S. Richter, M. Heinrich, S. Döring, A. Tünnermann, and S. Nolte, "Formation of femtosecond laser-induced nanogratings at high repetition rates," Appl. Phys. A **104**, 503–507 (2011).
16. F. Zimmermann, A. Plech, S. Richter, A. Tünnermann, and S. Nolte, "The onset of ultrashort pulse-induced nanogratings," Laser Photonics Rev. **10**, 327–334 (2016).
17. A. Rudenko, J.-P. Colombier, T. E. Itina, and R. Stoian, "Genesis of nanogratings in silica bulk via multipulse interplay of ultrafast photo-excitation and hydrodynamics," Adv. Opt. Mater. **9**, 2100973 (2021).
18. R. Grigutis, G. Tamošauskas, V. Jukna, A. Risos, and A. Dubietis, "Supercontinuum generation and optical damage of sapphire and YAG at high repetition rates," Opt. Lett. **45**, 4507–4510 (2020).
19. G. Cheng, K. Mishchik, C. Mauclair, E. Audouard, and R. Stoian, "Ultrafast laser photoinscription of polarization sensitive devices in bulk silica glass," Opt. Express **17**, 9515–9525 (2009).
20. R. Grigutis, V. Jukna, M. Navickas, G. Tamošauskas, K. Staliunas, and A. Dubietis, "Conical third harmonic generation from volume nanogratings induced by filamentation of femtosecond pulses in transparent bulk materials," Opt. Express **29**, 40633–40642 (2021).
21. R. Grigutis, V. Jukna, G. Tamošauskas, and A. Dubietis, "Broadband conical third harmonic generation in femtosecond filament-modified fused silica," Opt. Lett. **48**, 506–509 (2023).
22. Q. Liang, Y. Zhong, Z. Fan, H. Diao, V. Jukna, W. Chen, A. Houard, Z. Zeng, R. Li, and Y. Liu, "Optical transmission during mid-infrared femtosecond laser pulses ablation of fused silica," Appl. Surf. Sci. **471**, 506–515 (2019).
23. O. Bernard, A. Kraxner, A. Boukhayma, J. A. Squier, C. Enz, and Y. Bellouard, "Third-harmonic generation monitoring of femtosecond laser-induced in-volume functional modifications," Optica **10**, 774–782 (2023).
24. A. Šuminiene, V. Jukna, R. Šuminas, G. Tamošauskas, M. Vengris, and A. Dubietis, "LiSAF: an efficient and durable nonlinear material for supercontinuum generation in the ultraviolet," Lith. J. Phys. **60**, 215–222 (2020).
25. N. Garejev, I. Gražulevičiūtė, D. Majus, G. Tamošauskas, V. Jukna, A. Couairon, and A. Dubietis, "Third- and fifth-harmonic generation in transparent solids with few-optical-cycle midinfrared pulses," Phys. Rev. A **89**, 033846 (2014).
26. M. J. Weber, *Handbook of Optical Materials* (CRC Press, 2003).
27. K. D. Moll, D. Homoelle, A. L. Gaeta, and R. W. Boyd, "Conical harmonic generation in isotropic materials," Phys. Rev. Lett. **88**, 153901 (2002).
28. V. Vaičaitis, V. Jarutis, and D. Pentaris, "Conical third-harmonic generation in normally dispersive media," Phys. Rev. Lett. **103**, 103901 (2009).
29. L. Mateos, P. Molina, J. Galisteo, C. López, L. E. Bausá, and M. O. Ramírez, "Simultaneous generation of second to fifth harmonic conical beams in a two dimensional nonlinear photonic crystal," Opt. Express **20**, 29940–29948 (2012).